Regulation of cell distancing in peri-plaque glial nets by Plexin-B1 affects glial activation and amyloid compaction in Alzheimer's disease

Yong Huang, Minghui Wang, Shalaka Wahane, Mitzy Ríos de Anda, Lap Ho, Yuhuan Li, Sangjo Kang, Ryan Neff, Ana Kostic, Joseph Buxbaum, John F. Crary, Bin Zhang, Hongyan Zou, Roland H. Friedel

SUPPLEMENTAL TABLE

Supplemental Table S1 contains a list of differentially expressed genes from single cell RNA-sequencing data of astrocyte subcluster sc-1 between *APP/PS1and APP/PS1* PB1-KO genotypes.

SUPPLEMENTAL FIGURES

Supplemental Figures S1 – S10 on following pages.

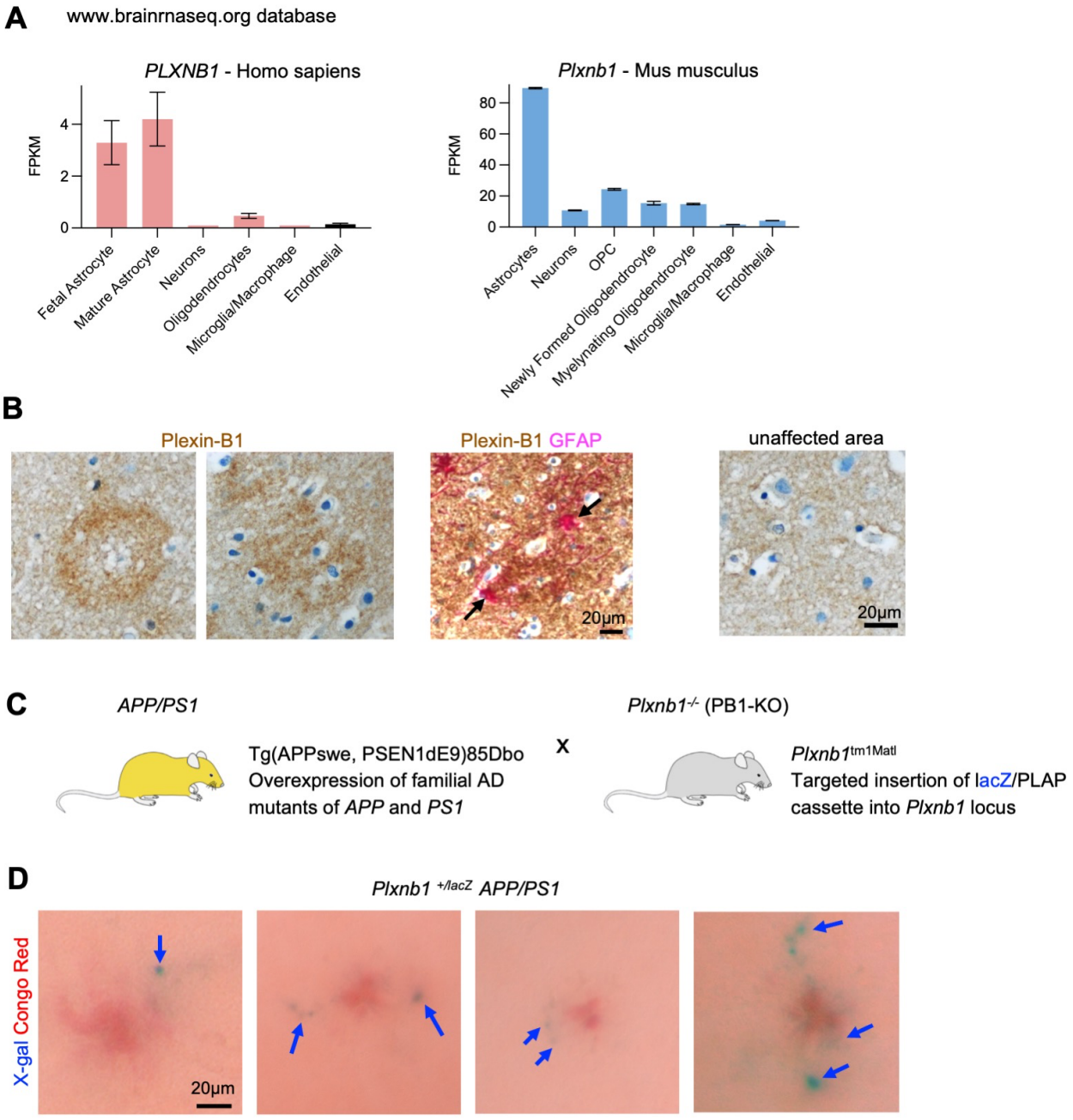

Figure S1. Plexin-B1 is predominantly expressed in astrocytes and upregulated near amyloid plaques.

A) RNA-seq data from both human and mouse brain cell types show that Plexin-B1 is predominantly expressed in astrocytes. Graphs compiled from data of www.brainrnaseq.org database.

B) Left, two additional examples of IHC images of post-mortem brain sections of AD patient (66 yrs old, neuropathology score A3B3C2) showing that Plexin-B1 is upregulated in corona-like patterns, presumably representing plaque-surrounding glial nets. Center, co-staining shows overlap of Plexin-B1 and GFAP (arrows) in reactive astrocytes. Right, low IHC signal for Plexin-B1in adjacent brain area not affected by plaques.

C) Amyloidogenic mouse line was crossed with Plexin-B1 KO line for experiments in this study.

D) Images of X-gal staining of cortex of *APP/PS1* $PB1^{+/lacZ}$ mice show that upregulation of lacZ is tightly associated with amyloid plaques, visualized with Congo Red. Four representative images are shown.

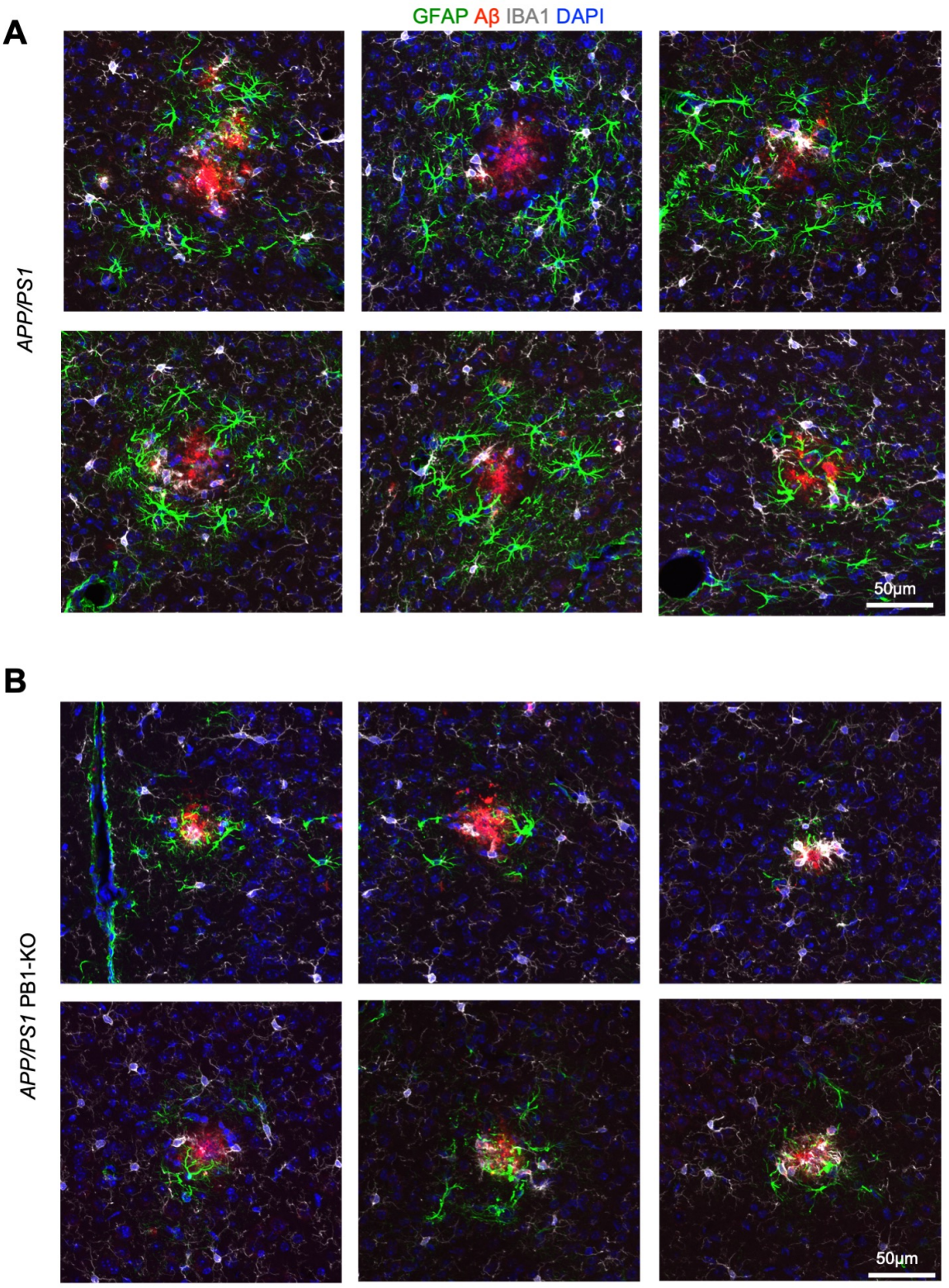

Figure S2. Smaller but more compact peri-plaque glial nets and higher glial coverage of plaques in *APP/PS1* PB1-KO mice.

A, B) Montage of IF images of plaques in cortex of *APP/PS1* and *APP/PS1* PB1-KO, each stained for amyloid plaques (6E10 antibody), and for reactive astrocytes and microglia (GFAP and Iba1, respectively). The montage is

composed of images taken from three different mice per genotype at 6 months. Note that PB1-KO resulted in fewer reactive astrocytes and activated microglia in the peri-plaque glial nets, but closer proximity of glial processes to Aβ plaques. Also note that Aβ plaques appeared more compact in *APP/PS1* PB1-KO.

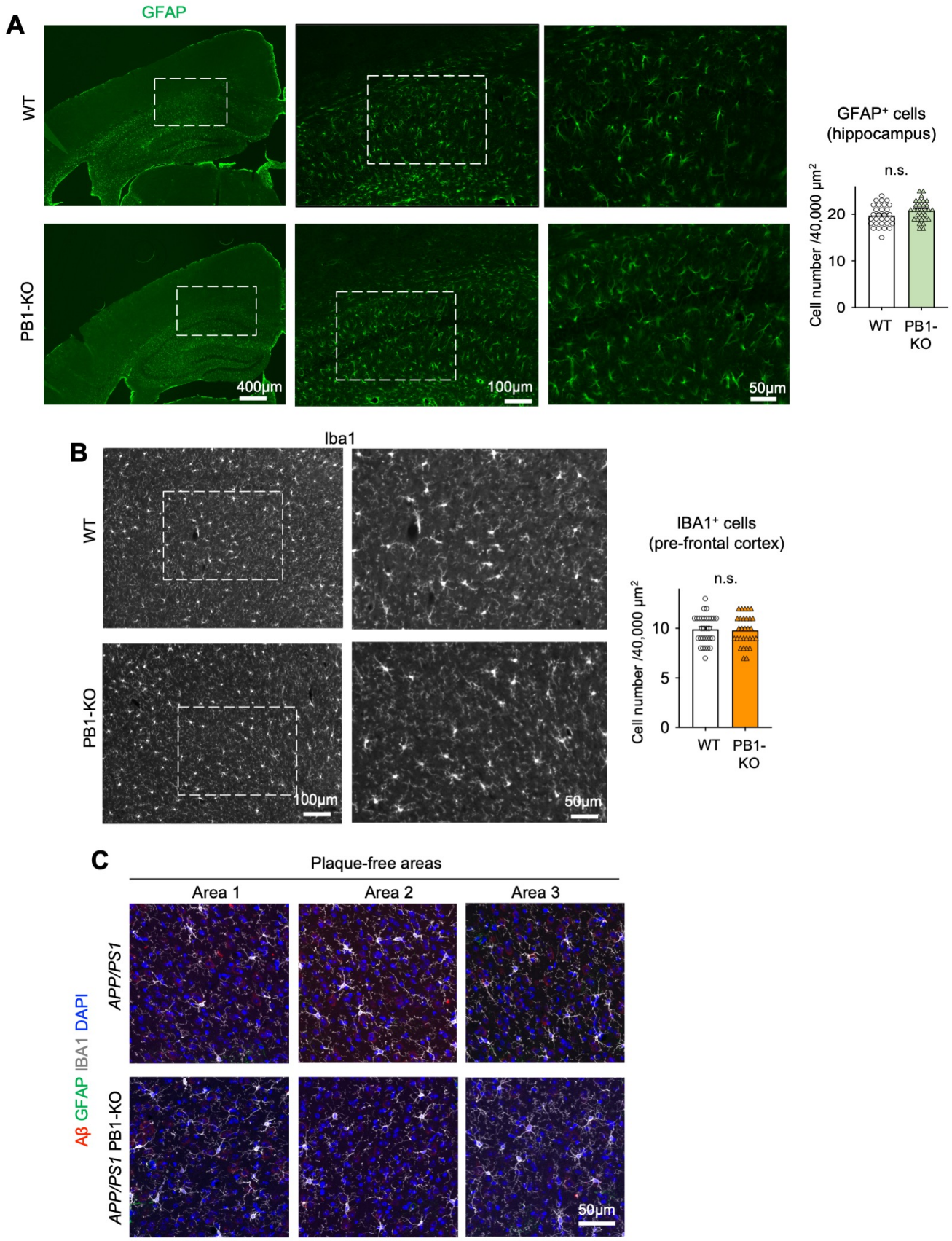

Figure S3. Homeostatic glial populations are not affected by Plexin-B1 ablation.

A) Density and distribution of $GFAP^+$ astrocytes in wild-type control and Plexin-B1 KO mouse brains (hippocampus) appeared similar. Unpaired *t*-test. n=30 areas for each genotype. n.s., not significant.

B) Density and distribution of $Iba1^+$ microglia in wild-type and Plexin-B1 KO mouse brains (pre-frontal cortex) appeared similar. Unpaired *t*-test. n=30 areas for each genotype. n.s., not significant.

C) Cortical areas in *APP/PS1* and *APP/PS1* PB1-KO mice that are unaffected by plaques had similar density of $Iba1^+$ cells. No $GFAP^+$ reactive astrocytes were detected in normal cortical areas.

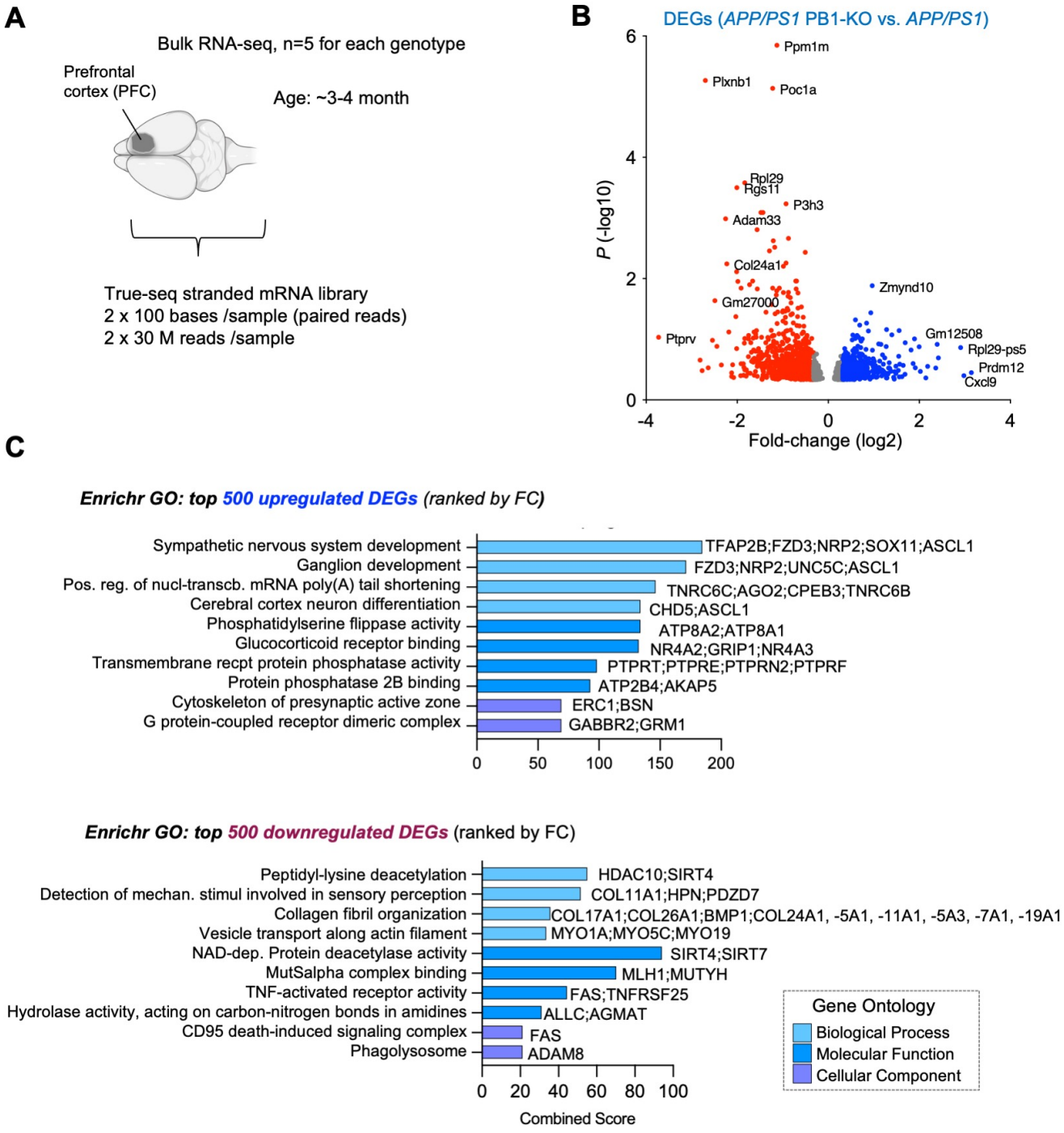

Figure S4. Transcriptomic analysis of cortical tissues from AD model mice with Plexin-B1 KO.

A) Experimental scheme of tissue-level (bulk) RNA-seq of prefrontal cortex (PFC) from 5 independent mice for each genotype (WT, PB1-KO, *APP/PS1*, *APP/PS1* PB1-KO).

B) Volcano plot showing DEGs (cut-off $P<0.05$) in PFC of *APP/PS1* vs. *APP/PS1* PB1-KO mice. Genes with >1.25-fold increase or decrease are labeled red or blue, respectively. Selected top DEGs are labeled with gene symbols.

C) Enrichr pathway enrichment analyses for gene ontologies (GO) of top 500 up- or down-regulated DEGs (ranked

by fold change) in PFC of *APP/PS1* PB1-KO vs. *APP/PS1*.

A

Raw data overview scRNA-seq			
CELL RANGER			
	No. of cells	Mean reads/cell	Median genes/cell
WT	5,856	105,883	1,198
PB1-KO	11,337	57,429	1,886
APP/PS1	9,837	59,376	1,200
APP/PS1 PB1-KO	6,942	88,352	1,786
sum	*33,972*		
Animals 6 months old, hippocampus			

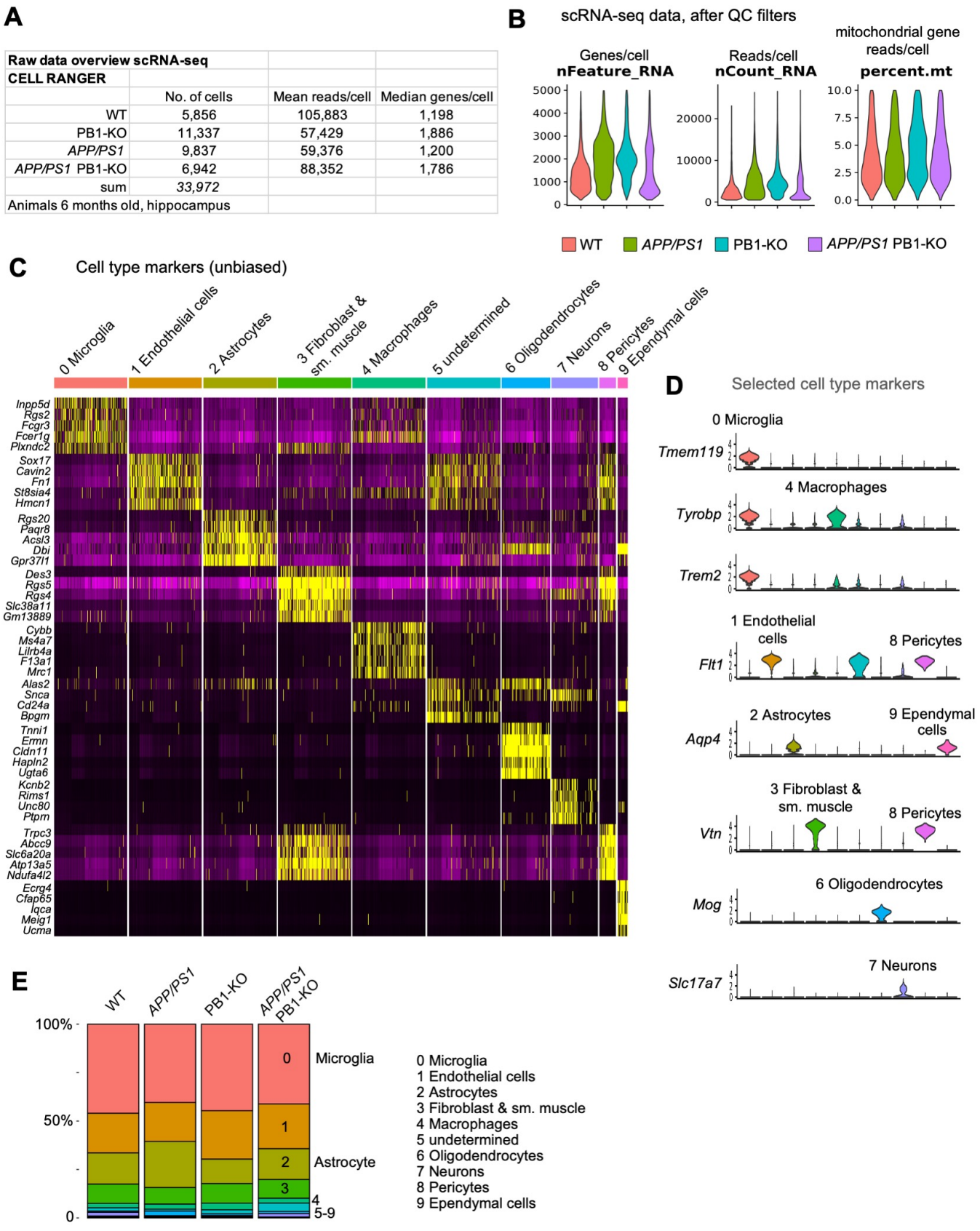

Figure S5. Single cell transcriptomic analysis of hippocampus shows 10 major cell type clusters.

A) Raw data cell numbers and sequence reads obtained from scRNA-seq using the10X Genomics system, as

presented by Cell Ranger analysis pipeline.

B) Gene and read numbers per cell after application of quality filters with Seurat package (see Methods for details).

C) Heatmap of marker genes expression in clusters 0 – 9. Cell type assignments are labeled on top.

D) Violin plots of gene expression of selected cell type specific marker genes in the clusters.

E) Relative proportions of cell type clusters in samples of different genotypes.

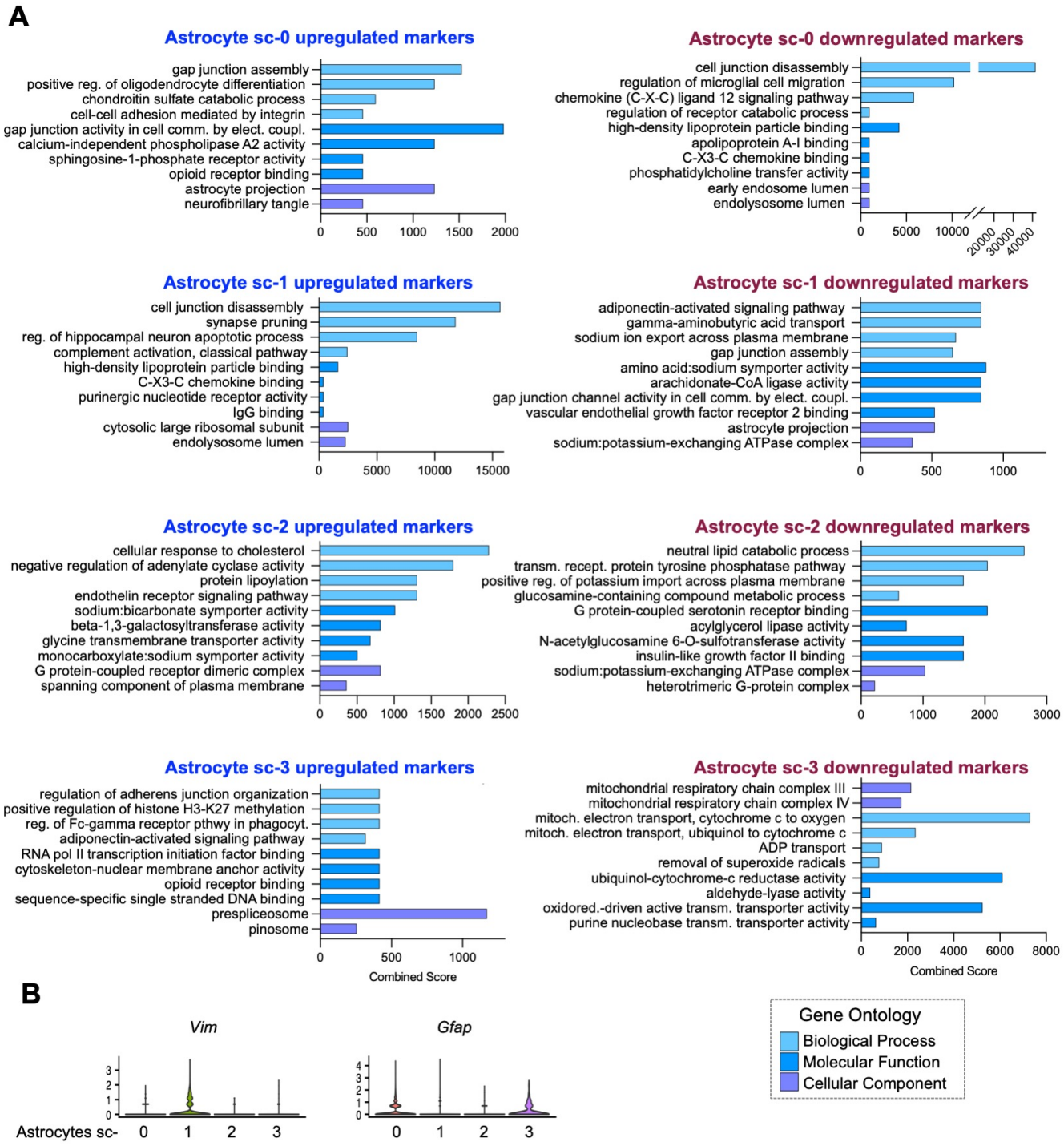

Figure S6. Characterization of transcriptomic profiles of astrocyte subclusters.

A) Gene ontology enrichment analysis of the differentially expressed marker genes in each astrocyte subclusters against one another. Up- and downregulated DEGs are analyzed separately.

B) Violin plots show expression pattern of vimentin and GFAP genes across astrocyte subclusters.

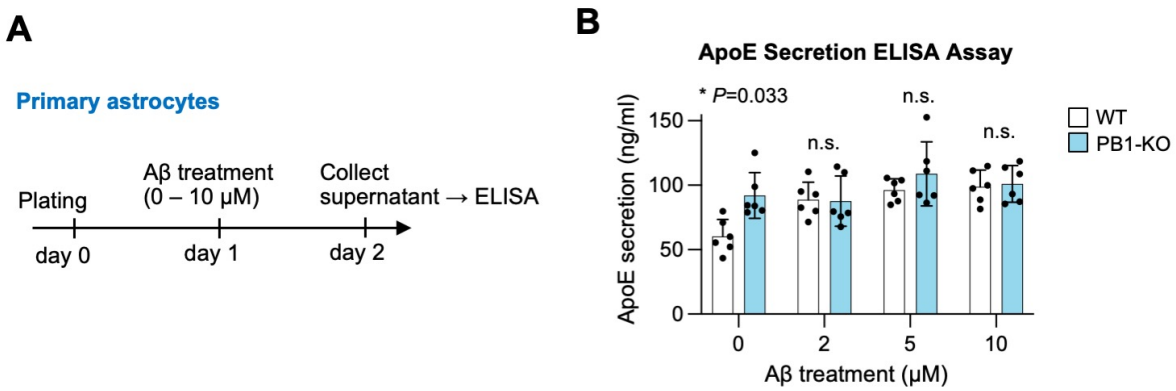

Figure S7. ApoE baseline secretion from primary astrocytes is increased by Plexin-B1 KO.

A) Experimental scheme. Primary astrocytes were derived from WT and PB1-KO mice and plated at 30,000 cells/well into 24 well plates (n=6 per condition). After one day, cells were treated with increasing concentrations of Aβ1-42 peptide. One day later, supernatants were collected to measure ApoE release.

B) ELISA assay results show that ApoE secretion was significantly higher in Plexin-B1 KO under baseline conditions without Aβ challenge. Aβ stimulation increased ApoE secretion from wildtype (WT) astrocytes, but did not further elevate the already high levels of ApoE secretion from Plexin-B1-deficient astrocytes. Each ELISA sample was measured with technical triplicates. n=6 independent cultures. Two-way ANOVA with Tukey's multiple comparison test.

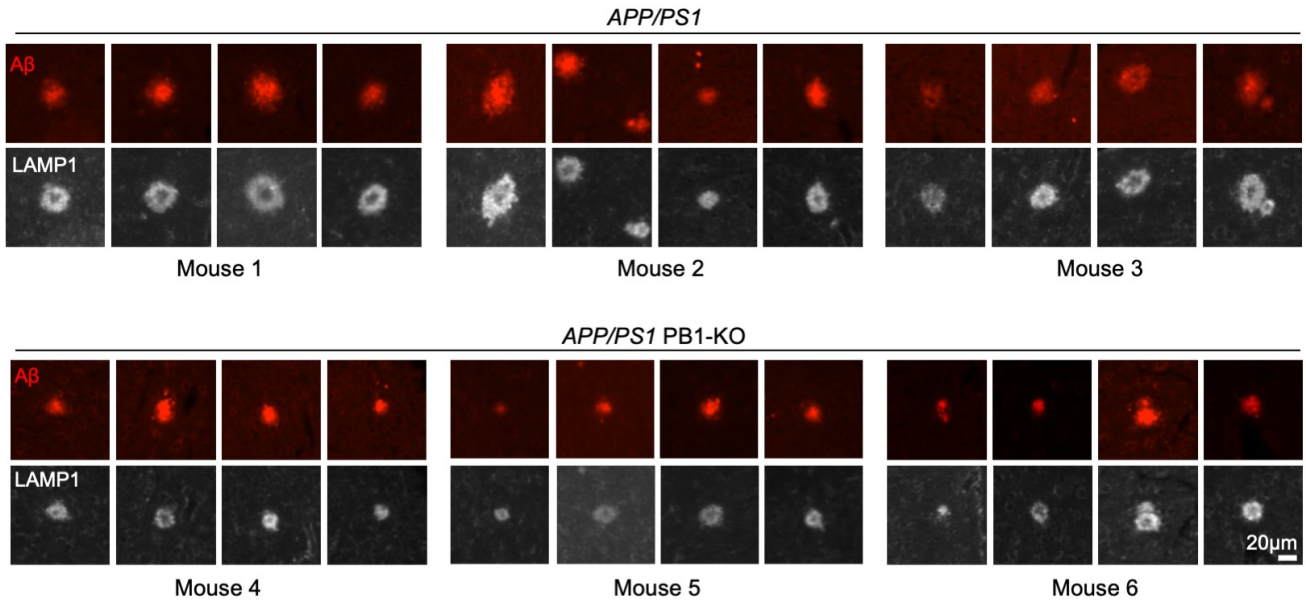

Figure S8. Plexin-B1 deletion results in reduced neuritic dystrophy around amyloid plaques.

Representative images from cortical brain sections of *APP/PS1* (top row) and *APP/PS1* PB1-KO animals (bottom rows) at 6 months of age, stained for Aβ (antibody 6E10) and LAMP1. Note a more compact appearance of Aβ plaques (shift towards dense-core type) and smaller $LAMP1^{+}$ areas in Plexin-B1 KO conditions. See Fig. 5 and Fig. 6 in main manuscript for quantifications.

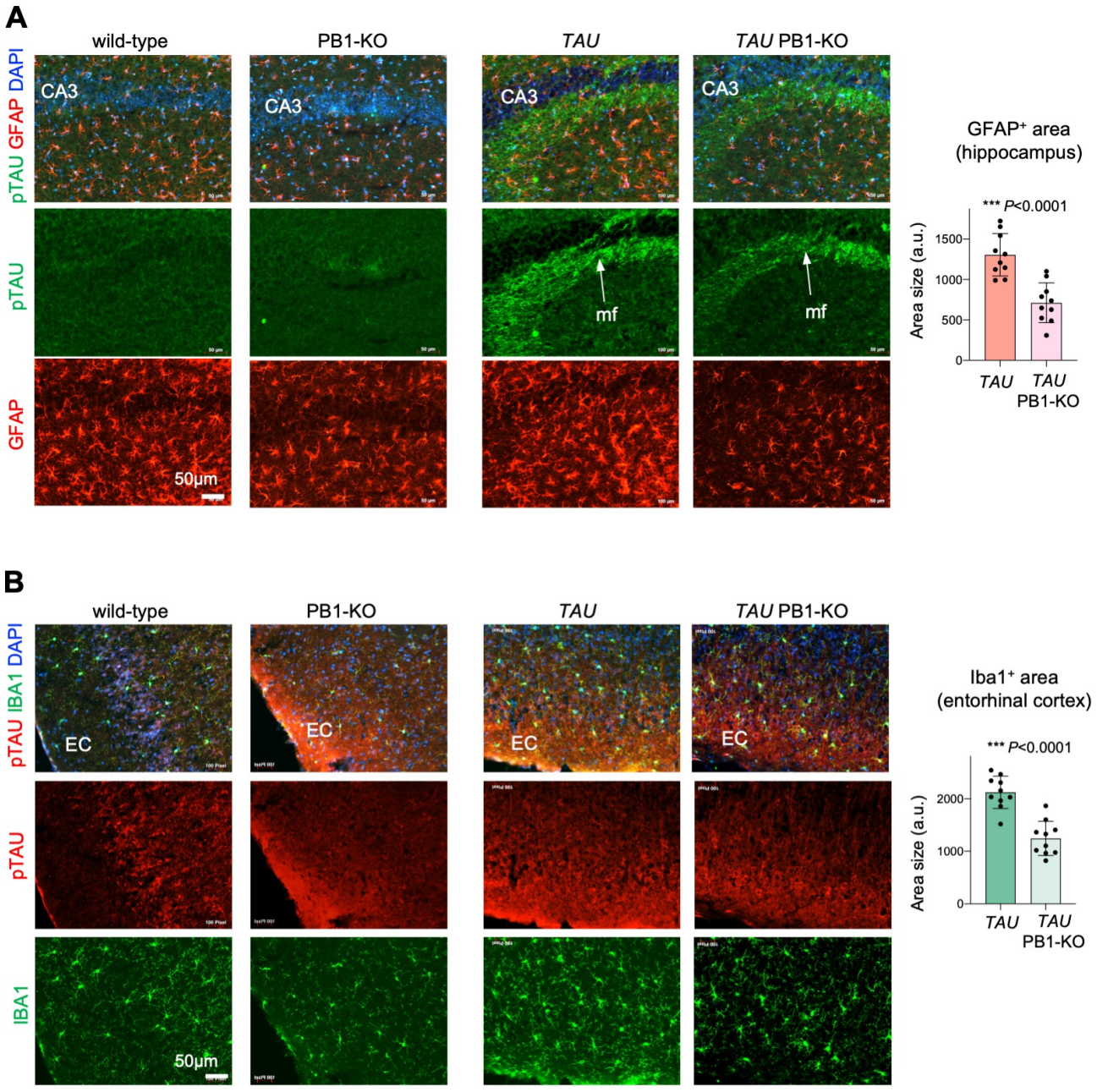

Figure S9. Attenuated gliosis in *TAU* model of neurodegeneration by Plexin-B1 KO.

A) IF images of hippocampus CA3 area of 3 month-old mice show accumulation of phospho-TAU (pTAU) and associated astrocyte reactivity (GFAP$^+$) in mossy fiber bundle (mf) in TAU mice (strain *TAU*-PS19), which were attenuated in *TAU* PB1-KO mice. Unpaired *t*-test. n=10 independent areas per genotype. a.u., arbitrary units.

B) IF images of entorhinal cortex (EC) show pTAU accumulation and associated microglial activation (Iba1$^+$)in *TAU* PB1-KO mice, which were reduced in *TAU* PB1-KO mice. Unpaired *t*-test. n=10 independent areas per genotype. a.u., arbitrary units.

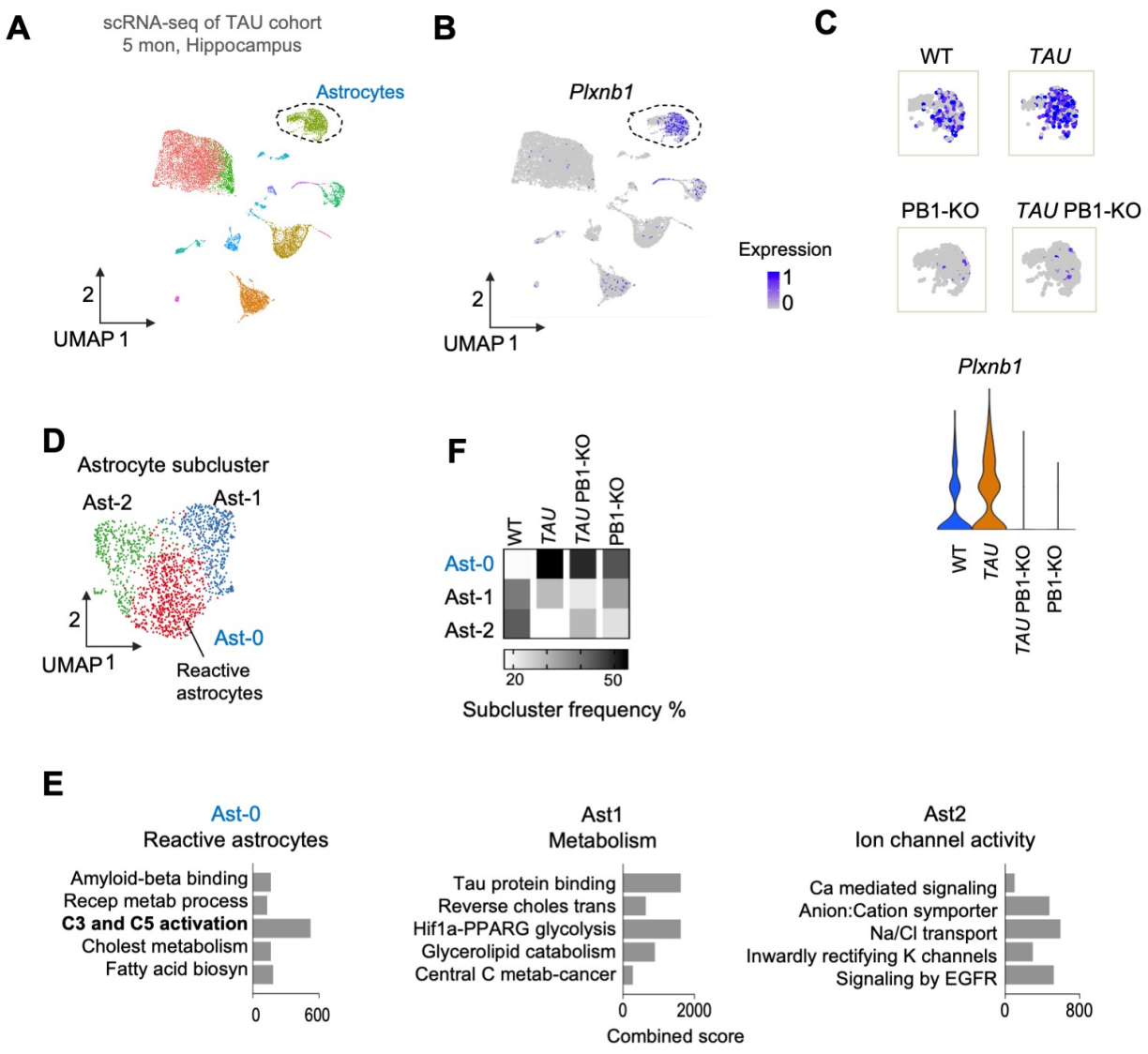

Figure S10. Single cell transcriptomics confirms attenuated astrocytosis in *TAU* model of neurodegeneration by Plexin-B1 KO.

A) UMAP representation of combined scRNA-seq data of hippocampus from 5 month-old mice (four genotypes: wild-type (WT), *TAU*, PB1-KO, *TAU* PB1-KO). Colors indicate different cell type clusters. Astrocytes, encircled by dashed line, are assigned by expression of marker genes (*Aqp4, Slc1a2, Aldoc*).

B) Expression of *Plxnb1* was mainly detected in astrocytes.

C) Expression of *Plxnb1* in astrocytes was increased in *TAU* compared to WT, and was ablated by PB1-KO, shown by feature plots and by violin plots, each split into the four genotypes.

D) Subclustering of astrocytes from hippocampal samples show three distinct astrocytic states. Subcluster Ast-0 contained reactive astrocytes, as assessed by DEG gene expression profiles (see below).

E) Gene ontology enrichment analysis of subcluster-specific marker genes. Note enrichment of genes associated with amyloid-beta binding, C3/C5 complement activation, and lipid metabolism in reactive Ast-0 subcluster. Ast-1 astrocytes are enriched for metabolic pathway genes and Ast-2 for genes related to ion channel activity.

F) Heatmap showing relative proportions of astrocytes subclusters in different genotypes. Note expansion of Ast-0 reactive astrocytes in *TAU* vs. wild-type sample (53.8% vs. 17.9%); this increase was reduced in *TAU* PB1 KO condition (49.3%). Also note increased proportion of Ast-0 in PB1-KO mice (44.3%) compared to WT.